Velocity oscillations in actin-based motility

2008 New J. Phys. 10 033022

(http://iopscience.iop.org/1367-2630/10/3/033022)

New Journal of Physics
The open-access journal for physics

Velocity oscillations in actin-based motility

Azam Gholami[1], **Martin Falcke**[1,3] **and Erwin Frey**[2]

[1] Hahn-Meitner-Institute, Department of Theoretical Physics, Glienicker Strasse. 100, 14109 Berlin, Germany
[2] Arnold Sommerfeld Center for Theoretical Physics and Center of NanoScience, Ludwig-Maximilians-Universität, Theresienstrasse 37, 80333 München, Germany
E-mail: falcke@hmi.de

New Journal of Physics **10** (2008) 033022 (12pp)
Received 10 October 2007
Published 12 March 2008
Online at http://www.njp.org/
doi:10.1088/1367-2630/10/3/033022

Abstract. We present a simple and generic theoretical description of actin-based motility, where polymerization of filaments maintains propulsion. The dynamics is driven by polymerization kinetics at the filaments' free ends, crosslinking of the actin network, attachment and detachment of filaments to the obstacle interface and entropic forces. We show that spontaneous oscillations in the velocity emerge due to a push–pull mechanism in a broad range of parameter values, and compare our findings with experiments.

Contents

[3] Author to whom any correspondence should be addressed.

1. Introduction

The ability to move is essential for living cells to survive. It may be used in the search for nutrients, such as the motion of the amoeba *Dictyostelium discoideum*, or for the purpose of reaching another host for pathogens moving inside and between host cells. In both cases, cells face the task of turning chemical energy into linear motion. They have developed a mechanism exploiting the polarity of actin polymers, which prefer to bind monomers at one end and preferentially release them at the other end. Actin is present in abundance in eukaryotic cells and forms semiflexible polymers belonging to the cytoskeleton. Bacteria hijack the actin polymerization machinery of host cells for their own purposes.

Force generation by semiflexible actin polymers is also used for cell motility in many other eukaryotic cells and is crucial for development, regeneration, wound healing and the immune response. The force exerted by the filaments arises from *elastic and entropic* contributions since semiflexible polymers undergo thermal shape fluctuations [1, 2]. This generates propulsion in combination with polymerization. Thus, the leading edge of lamellipodia of crawling cells [3] is pushed forward by a polymerizing actin meshwork and bacteria move inside cells by riding on a comet tail of growing actin filaments [4, 5]. These *in vivo* systems of actin-based motility are complemented by *in vitro* assays using plastic beads, lipid vesicles and oil droplets [6]–[11].

Polymerization at the surface of the obstacle generates motion. The same process produces the filaments which form the actin meshwork further back from the surface. The meshwork provides the support required for exerting a force on the obstacle. Complete understanding of cell motility or pathogen propulsion requires consideration of both the meshwork dynamics and the force generation and polymerization dynamics close to the obstacle surface in the so-called polymer brush. A macroscopic theory for the meshwork as an active gel was developed recently [12]–[14]. Here, we focus on the dynamics of polymerization and force generation.

Mathematical models have quantified the force generated by actin filaments growing against obstacles [1, 2, 15]. The resisting force depends on the obstacle which is pushed. In the case of pathogens, it consists mainly of the force exerted by actin filaments bound to the surface of the bacterium and pulling it backwards [16, 17]. The tethered ratchet model [18] is a mathematical formulation of these experimental findings. It focuses on the dynamics of the number of attached and detached polymers. In contrast with that, we will start from the dynamics of distributions of the free length of the polymer.

Actin polymerization is controlled by a complex molecular network [5]. Nucleation of new filaments, capping of existing ones, exchange of ADP for ATP on actin monomers, buffering of monomers, etc all contribute to that control and have been modeled [18]–[20]. Our goal is not to model the full complexity of that biochemical network. We rather focus on the core process of force generation and force balance resulting from the interplay between bound pulling filaments and polymerizing pushing filaments, the transition between these two groups and the motion of the whole force-generating configuration. This is motivated by recent observations of complex dynamics in simple reconstituted systems: the velocity of beads, pathogens or oil droplets propelled by actin polymerization may oscillate [11], [21]–[23]. Our goal is to describe the dynamics of such biochemically simpler systems and find a robust microscopic description for oscillation mechanisms, which may then be controlled by higher order processes.

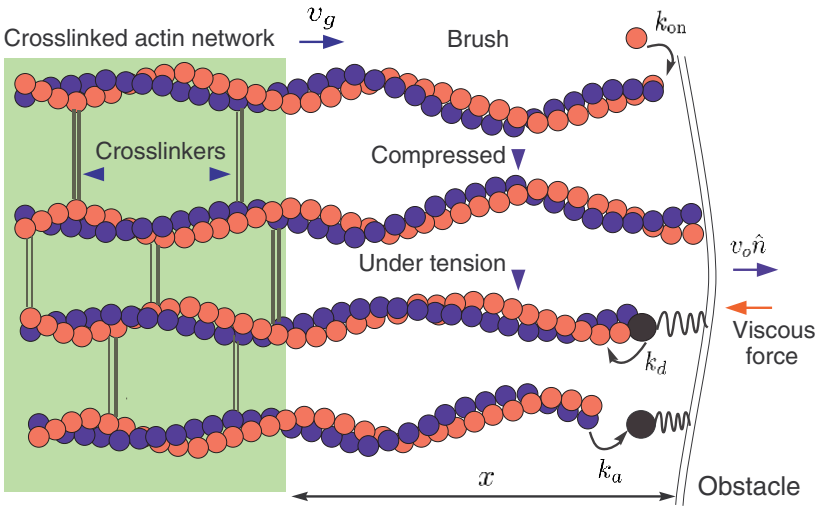

Figure 1. Schematic representation of an ensemble of actin filaments in the brush oriented at $\vartheta = 0$ with respect to the normal $\hat{n}$ of an obstacle interface. While attached filaments are under tension and pull the interface back, detached filaments are compressed, polymerize with rate k_{on} and push the interface forward. All filaments are firmly anchored in a crosslinked meshwork, whose front advances with velocity v_g reducing the free contour length l of the filaments in the brush. Attached filaments detach with stress dependent rate k_d and detached filaments attach with constant rate k_a. v_o is the interface velocity in the extracellular medium, and x is the distance between the front of the meshwork and the interface.

We will describe the model in the following section. Section 3 describes the results of simulations and bifurcation analyses and section 4 will relate our results to experiments and to previous work on simple models of actin-based motility.

2. A simple model of actin-based motility

The dynamics of the total number of filaments N are due to nucleation of new filaments and capping of existing ones. Capped filaments stop polymerizing and drop out of the dynamics. But to keep matters simple and based on the assumption that nucleation and capping balance we neglect N-dynamics. We consider a fixed number N of actin filaments. It was shown experimentally by Brieher *et al* [24] that propulsion with a constant number of filaments is possible, although the authors did not report saltatory motion. The fixed number of filaments implies that we will not reproduce changes in F-actin density in actin comet tails as reported to be associated with saltatory motion [11, 22].

The filaments are firmly anchored into a rigid crosslinked meshwork, which advances with velocity v_g; for an illustration see figure 1. We consider the processes in the polymer brush between the crosslinked meshwork and the surface of the obstacle which is pushed by actin polymerization. Severing and depolymerization can be neglected for the brush dynamics according to experimental ideas on processes in actin comet tails and lamellipodia [25].

Filaments of variable free length l are either attached to the obstacle surface via a protein complex or detached from it. The two populations are specified by time-dependent number distributions denoted $N_a(l,t)$ and $N_d(l,t)$, respectively. Filaments in the detached state polymerize with a velocity $v_p(l,x)$, which depends on both the polymer length l and the distance x between rigid support and obstacle. The constant attachment rate k_a and a stress-dependent detachment rate k_d [26] describe the transitions between the two filament populations. Attachment occurs during nucleation of new filaments. They nucleate from activated Arp2/3 which is activated and inserted into existing filaments by protein complexes bound to the obstacle surface including e.g. ActA and WASP (see the review [25] and references therein). While we consider the total number of filaments to be constant, we do not neglect this transient attachment aspect of nucleation. Another putative transient attachment is mediated by the isolated WH2 domain of N-WASP which forms a complex with G-actin. This complex can bind barbed ends and mediates their binding to the bacterium ([25, 27] and references therein). We lump both attachment processes into one rate law since both rates are proportional to $N_d(l,t)$.

The evolution of the length distributions $N_a(l,t)$ and $N_d(l,t)$ obeys an advection–reaction equation:

$$\frac{\partial}{\partial t}N_d - \frac{\partial}{\partial l}\left[\max\left(\frac{l}{x},1\right)v_g(l) - v_p\right]N_d = -k_a N_d + k_d N_a, \tag{1a}$$

$$\frac{\partial}{\partial t}N_a - \frac{\partial}{\partial l}\left[\max\left(\frac{l}{x},1\right)v_g(l)\right]N_a = k_a N_d - k_d N_a. \tag{1b}$$

The right-hand side of equations (1) describes attachment and detachment processes. The second term on the left-hand side accounts for the gain and loss of the free length of the polymer due to the dynamics of the polymer mesh, growing with velocity v_g, and the polymerization kinetics of the filaments in the brush v_p. The graft velocity v_g has the direction orthogonal to the graft boundary. This is not the tangential direction of polymers if polymers are bent or tilted. However, the advection term in equations (1) requires velocities along the contour of filaments. The correction factor $\max(\frac{l}{x},\ 1)$ turns v_g into such a velocity, i.e. the rate with which the graft swallows contour length. It was derived with the assumption that filaments extend all the way from the graft to the obstacle wall which is the case with precision sufficient for this purpose (see section 3).

The graft point represents the boundary between the polymer brush and the bulk gel of the actin comet tail [28]. Consequently, the complete description of the motion of the graft would require solving the bulk gel equations for the comet tail [12]. However, this would be far beyond the purpose of this project, which focuses on processes in the polymer brush very much in the spirit of the tethered ratchet model [18]. The coupling between the obstacle surface and gel boundary we assume here entails a graft velocity independent of the obstacle velocity at large polymer length ($l \gg \bar{l}$, see below) and a graft velocity equal to the obstacle velocity at small polymer length, i.e. when the brush disappears.

Processes contributing to the growth of the rigid polymer mesh are entanglement and crosslinking of filaments in the brush. Both imply a vanishing v_g for $l \to 0$, since short polymers do not entangle and crosslinking proteins are unlikely to bind to them. At the same time v_g

cannot grow without bound but must saturate at some value v_g^{max} due to rate limitations for crosslinking and entanglement. This suggests taking the following sigmoidal form:

$$v_g(l) = v_g^{max} \tanh(l/\bar{l}) , \tag{2}$$

with a characteristic length scale $\bar{l}$. The constant $\bar{l}$ could be perceived as the width of the brush gel boundary.

The polymerization rate is proportional to the probability of a gap of sufficient size d ($\approx$2.7 nm) between the polymer tip and the obstacle for insertion of an actin monomer as was calculated in [1]. This implies an exponential dependence of v_p on the force F_d by which the polymer pushes against the obstacle,

$$v_p(l, x) = v_p^{max} \exp[-d \cdot F_d(l, x)/k_B T] . \tag{3}$$

Here, $v_p^{max} \approx 500\,\mathrm{nm\,s^{-1}}$ [1] is the force-free polymerization velocity. For the entropic force F_d we use the results obtained in [2] for $D = 2$ and 3 spatial dimensions, where we take the accepted value of $\ell_p \approx 15\,\mu$m [29, 30] for the persistence length of F-actin.

The dynamics of the distance x between the grafted end of the filament and the obstacle interface (see figure 1) is given by the difference of the average v_g and the velocity of the obstacle

$$\partial_t x = -\frac{1}{N}\int_0^\infty \mathrm{d}l\, v_g(l)\,[N_a(l,t) + N_d(l,t)] + \frac{1}{\zeta}\int_0^\infty \mathrm{d}l\,[N_a(l,t)F_a(l,x) + N_d(l,t)F_d(l,x)] , \tag{4}$$

where ζ is an effective friction coefficient of the obstacle. Note that $|F_a|, |F_d| \gg \zeta v_o$ holds, with v_o denoting the obstacle velocity. The polymerization force and the force exerted by bound filaments dominate the force balance in agreement with experimental results reported in [31].

The force $F_a(l, x)$ acting on the obstacle interface results from the compliance of the filaments attached to it by some linker proteins. We model these proteins as springs with spring constant k_l and zero equilibrium length. This complex has a nonlinear force–extension relation which we approximate by a piece-wise linear function; for details see the supplementary material (available from stacks.iop.org/NJP/10/033022/mmedia). Let $R_\parallel \approx l[1 - l(D-1)/4\ell_p]$ be the average distance from the graft point to the tip of the filament projected onto the grafting direction. The elastic response of filaments experiencing small compressional forces ($x \leqslant R_\parallel$) is approximated by a spring constant $k_\parallel = 12 k_B T \ell_p^2/(D-1)l^4$ [32]. For small pulling forces ($x \geqslant R_\parallel$), the linker–filament complex acts like a spring with an effective constant $k_{eff} = k_l k_\parallel/(k_l + k_\parallel)$. In the strong force regime, the force–extension relation of the filament is highly nonlinear and diverges close to full stretching [33]. Therefore, only the linker will stretch out. The complete force–extension relation is captured by

$$F_a = \begin{cases} -k_\parallel(x - R_\parallel) , & x \leqslant R_\parallel , \\ -k_{eff}(x - R_\parallel) , & R_\parallel < x < l , \\ -k_l(x - l) - k_{eff}(l - R_\parallel) , & x \geqslant l . \end{cases} \tag{5}$$

Finally, we specify the force dependence of the detachment rate according to [26] by

$$k_d = k_d^0 \exp[-d \cdot F_a(l, x)/k_B T] \tag{6}$$

with $k_d^0 \approx 0.5\,\mathrm{s^{-1}}$ [18].

Equation (1*a*) has a singularity at $v_p(l_s) = \max(1, l_s/x)\, v_g(l_s)$ since the coefficient of the derivative of N_d with respect to l is zero at l_s. The existence of this singularity sets the

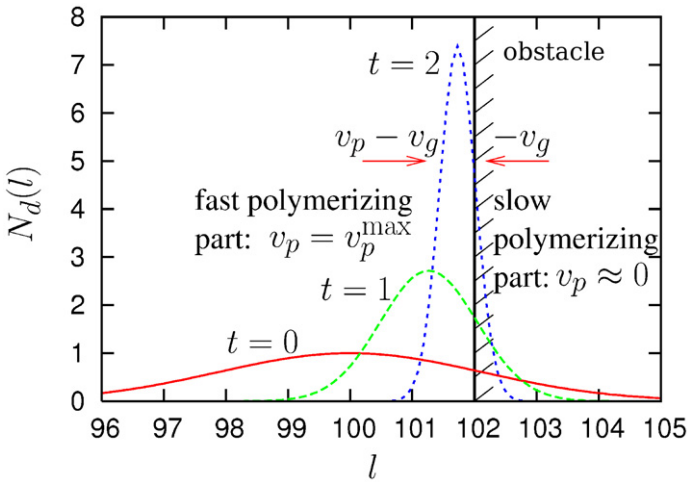

Figure 2. The evolution of the solution of equation (7). The width of the initial Gaussian distribution of detached filaments decreases exponentially with time and the peak of the distribution grows and localizes around l_s. In the full system, l_s is close to x since v_p drops from $v_p^{\max}$ to almost 0 in a narrow range around $l = x$.

length distribution dynamics of equation (1*a*) apart from distribution dynamics of polymers in solution [34, 35]. To illustrate the key physical features at that singularity, we start with the simple equation $\partial_t N_d - \partial_l[\max(1, l/x)v_g(l) - v_p(l, x)]N_d = 0$ with x kept constant. Then, those parts of the distribution of N_d with $l < l_s$ will grow and catch up with l_s since $\max(1, l/x)v_g(l) - v_p(l, x)$ is positive there, while the parts with $l > l_s$ will shorten towards l_s. As a consequence, the whole distribution will become concentrated at l_s. To quantify this heuristic argument, we expand $\max(1, l/x)v_g(l) - v_p(l, x)$ up to linear order around l_s like $v_1(l - l_s)$ and obtain the advection equation

$$\frac{\partial}{\partial t} N_d - \frac{\partial}{\partial l} [v_1(l - l_s)] N_d = 0 , \tag{7}$$

which we solve by the method of characteristics. Starting initially with a Gaussian distribution we obtain $N_d(l, t) = c(t) \exp[-(l - \bar{l}(t))^2/w(t)^2]$ with $c(t) = c_0 \exp(v_1 t)$, $\bar{l}(t) = l_s + (\bar{l}_0 - l_s) \exp(-v_1 t)$ and $w(t) = w_0 \exp(-v_1 t)$. This shows that N_d evolves to a monodisperse distribution which is localized around l_s. Its width decreases exponentially with time while its height grows exponentially. The timescale for this contraction is given by $[\partial_l(\max(1, l/x)v_g - v_p)]^{-1}$ and is in the range of 10^{-2} s (for details see the supplementary material, available from stacks.iop.org/NJP/10/033022/mmedia). This is 1–2 orders of magnitude faster than any other time constant of the system. The temporal evolution of the solution of equation (7) is shown in figure 2. Since the same kind of singularity also occurs in the full set of dynamic equations, equations (1*a*) and (1*b*), we may readily infer that N_a and N_d evolve into delta-functions with that dynamics. This is well supported by simulations, and allows us to continue with the ansatz

$$N_d(l, t) = n_d(t)\delta(l - l_d(t)) , \tag{8a}$$

$$N_a(l, t) = n_a(t)\delta(l - l_a(t)) . \tag{8b}$$

It defines the dynamic variables $n_d(t)$, $l_d(t)$, $n_a(t)$ and $l_a(t)$. Upon inserting equations (8*a*) and (8*b*) into (1) and (4), multiplying (1) and (4) by l and integrating over l, we obtain

$$\partial_t l_d(t) = v_p(l_d, x) - \max\left(\frac{l_d}{x}, 1\right) v_g(l_d) + k_d \frac{n_a}{n_d}(l_a - l_d), \tag{9a}$$

$$\partial_t l_a(t) = -\max\left(\frac{l_a}{x}, 1\right) v_g(l_a) + k_a \frac{n_d}{n_a}(l_d - l_a), \tag{9b}$$

$$\partial_t n_a(t) = -k_d(l_a, x) n_a(t) + k_a n_d(t), \tag{9c}$$

$$\partial_t x(t) = \frac{1}{\zeta}\left[n_a(t) F_a(l_a, x) + n_d(t) F_d(l_d, x)\right] - \frac{1}{N}\left[v_g(l_a) n_a(t) + v_g(l_d) n_d(t)\right], \tag{9d}$$

where $n_d(t) = N - n_a(t)$, since we keep the total number of filaments fixed. The most obvious differences between these equations and the tethered ratchet model are the dynamics of $x(t)$, $l_d(t)$ and $l_a(t)$ [18].

The values of many parameters of equations (9) can be estimated using known properties of actin filaments. We choose the linker spring constant $k_l \approx 1\,\mathrm{pN\,nm^{-1}}$ [18] and assume $N = 200$ [18] filaments to be crowded behind the obstacle. A realistic value of the drag coefficient ζ is $10^{-3}\,\mathrm{pN\,s\,nm^{-1}}$ but results did not change qualitatively for a range from 10^{-5} to $1\,\mathrm{pN\,s\,nm^{-1}}$.

3. Results

We have numerically solved equations (9) in both $D = 2$ and 3 dimensions, and found the dynamic regimes shown in figure 3: *stationary states and oscillations*. The existence of an oscillatory regime is very robust against changes of parameters within reasonable limits including the spatial dimension. We checked robustness against changes in the parameter values for $N, \bar{l}$ (see equation (2)), k_l, ζ and k_d^0, in addition to the examples shown in figure 3. In general, we find that oscillations occur for $v_g^{\max} \lesssim 500\,\mathrm{nm\,s^{-1}}$ and within a range of values for k_a. Figure 3(d) demonstrates that changing $v_p^{\max}$ leads to a transition from steady to saltatory motion. $v_p^{\max}$ can be controlled by the concentration of free G-actin in experiments.

Oscillations are found for $v_g^{\max} < v_p^{\max}$ only. Otherwise, the graft catches up with the obstacle and stays very close to it resulting in motion with constant velocity. Starting at $k_a = 0$, we find an onset of oscillations upon increasing k_a at the lower boundary of the oscillatory region. The stationary state changes stability slightly inside the oscillatory regime and oscillations set in with a finite period and an amplitude different from 0; compare the example shown in figure 4(a). That is compatible with a saddle node bifurcation of limit cycles. A transition from steady to oscillatory motion upon increasing protein concentration in the extract is experimentally observed with beads [23]. An increase of protein concentration would also increase the binding rate k_a. Therefore, we assume that the onset of oscillations observed in these experiments corresponds to the lower transition line in figures 3(a)–(c), in particular since the measured oscillations start also with a large amplitude and finite period and the coexistence of steady and oscillatory motion close to the transition reported in [23] is reproduced by the model (we assume a subcritical Hopf bifurcation in the model, see [36]). The upper boundary of the oscillatory region is determined by a Hopf bifurcation. An example of an oscillation close to that bifurcation is shown in figure 4(b). Onset of oscillations in actin-based motility of

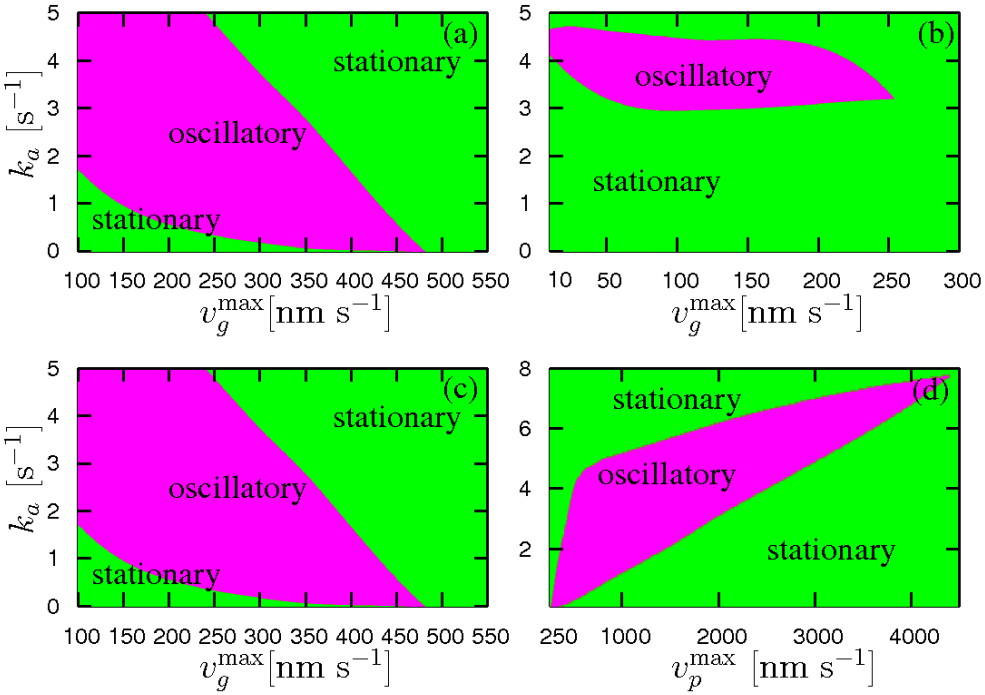

Figure 3. Phase diagram of equations (9) outlining stationary and oscillatory regimes with $v_{\mathrm{p}}^{\max} = 500\,\mathrm{nm\,s^{-1}}$ for (a)–(c) and (a) $D = 2$, $\vartheta = 0$, (b) $D = 2$, $\vartheta = \pi/4$, (c) $D = 3$, $\vartheta = 0$, and (d) $D = 3$, $\vartheta = 0$, $v_{\mathrm{g}}^{\max} = 250\,\mathrm{nm\,s^{-1}}$. $\zeta = 10^{-3}\,\mathrm{pN\,s\,nm^{-1}}$ and $\bar{l} = 100\,\mathrm{nm}$, all other parameter values are specified in the text.

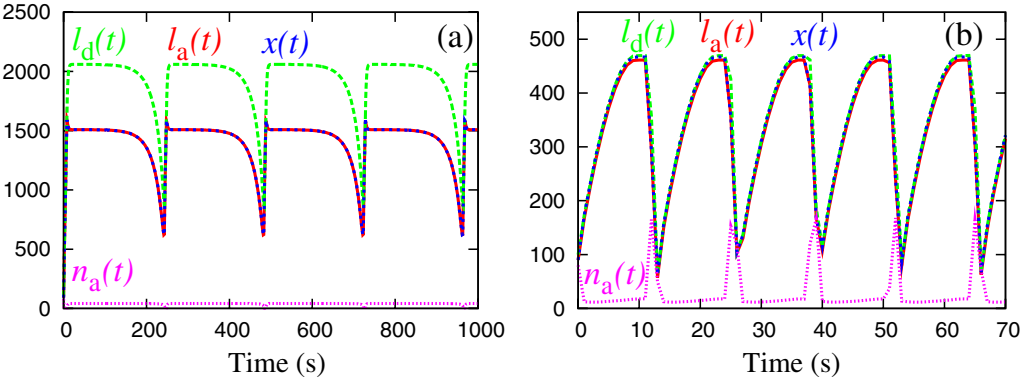

Figure 4. x, l_{a}, l_{d} (in nm) and n_{a} as a function of time, as obtained from numerical solutions of equations (9) with $v_{\mathrm{g}}^{\max} = 300\,\mathrm{nm\,s^{-1}}$ and (a) $k_{\mathrm{a}} = 0.143\,\mathrm{s^{-1}}$ and (b) $k_{\mathrm{a}} = 3.49\,\mathrm{s^{-1}}$. $D = 3$, $\bar{l} = 100\,\mathrm{nm}$ in both panels.

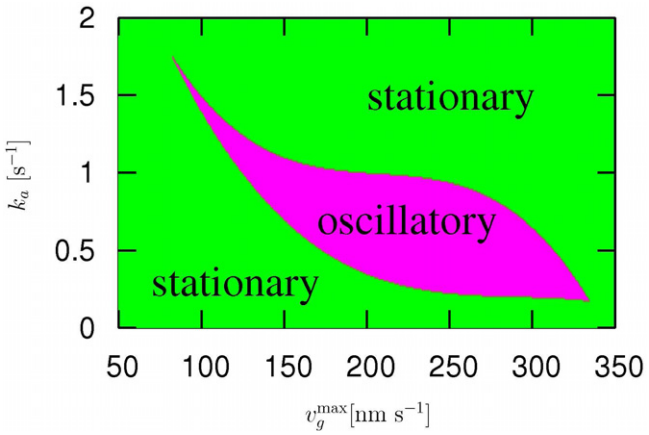

Figure 5. Phase diagram of a brush with two populations of filaments, one oriented at 0° and the other one at ±45°, outlining oscillatory and stationary regimes in $D = 3$. Other parameter values are the same as in figure 3(c).

oil droplets upon adding VASP to the medium is reported in [11]. The authors explain this onset by de-adhesion activity of VASP which could not be specified on the molecular level. The bifurcation diagram in figure 3 suggests that this onset of oscillations corresponds to the upper transition with an emergence of oscillations upon decreasing k_a. This bifurcation line can also be crossed by increasing the dissociation rate k_d^0, which would correspond to a different way of de-adhesion activity (data not shown). More details on the phase diagram will be published elsewhere [36].

We have also studied the system when the network is oriented at an angle $\vartheta = \pi/4$. In this case, the spring constant of the attached filaments parallel to $\hat{n}$ for $D = 2$ reads $k_\parallel^{-1}(\vartheta) = 4\ell_p^2[\frac{\epsilon}{2} + e^{-\epsilon/2} - 1 + \cos 2\vartheta(\frac{1}{4} + \frac{1}{12}e^{-2\epsilon} - \frac{1}{3}e^{-\epsilon/2}) - \cos^2\vartheta(e^{-\epsilon/2} - 1)^2]/k_BT$, where $\epsilon = l/\ell_p$ and $R_\parallel(\vartheta) = l(1 - l/4\ell_p)\cos\vartheta$ [32]. For the pushing force of a filament grafted at $\vartheta = \pi/4$, we use the results of the factorization approximation given in [2], which is valid for a stiff filament-like actin. A numerical solution of equations (9) with the adapted forms of F_d and F_a results in the phase diagram shown in figure 3(b).

Experimentally observed actin meshworks exhibit a range of filament orientations and therefore oscillations should work with filaments of different orientations in the brush. Their dynamics is coupled by the obstacle. Figure 3(b) shows the oscillatory regime of a network with filaments at ±45° in two dimensions (2D). Results of simulations modeling a brush with filaments with angles of 0° and ±45° in 3D are shown in figure 5. Such a brush oscillates also. These results imply that a brush comprising orientations between −45° and +45° would oscillate as well, since the overlap of the oscillatory regimes of tilted and orthogonal filaments increases with decreasing $|\vartheta|$.

We start with the description of the push–pull mechanism of the oscillations in the phase with $v_g > v_p$, i.e. decreasing lengths x, l_a and l_d; see figure 4(a). The magnitude of pulling and pushing forces increases due to their length dependence. When the pushing force becomes too strong, an avalanche-like detachment of attached filaments is triggered and the obstacle jerks forward; compare the steep rise in l_d, l_a and x shown in figure 4(a). That causes a just as sudden drop in the pushing force. With low pushing force now, polymerization accelerates and

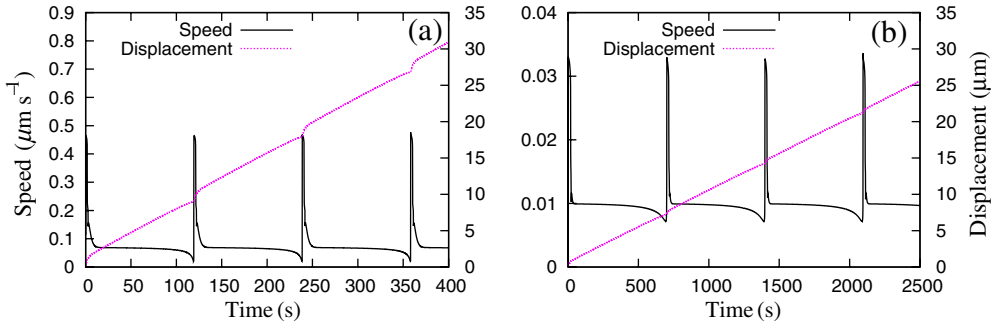

Figure 6. Velocity and displacement of the obstacle as a function of time with (a) $k_a = 0.525\,s^{-1}$, $v_p^{max} = 500\,nm\,s^{-1}$ and $v_g^{max} = 75\,nm\,s^{-1}$, (b) $k_a = 0.235\,s^{-1}$, $v_p^{max} = 40\,nm\,s^{-1}$ and $v_g^{max} = 10\,nm\,s^{-1}$. In both panels $k_d^0 = 0.1\,s^{-1}$, $\bar{l} = 100\,nm$, $\zeta = 10^{-3}\,pN\,s\,nm^{-1}$ and $D = 3$.

increases the length of detached filaments. The restoring force of attached filaments is weak in this phase due to their small number. Hence, despite the fact that there are no strong pushing forces, the obstacle moves forward. In the meantime, some detached filaments attach to the surface such that the average length and number of attached filaments increases as well. When the detached filaments are long enough to notice the presence of the obstacle interface, they start to buckle. This, in turn, increases the pushing force and slows down the polymerization velocity. Therefore, the graft velocity now exceeds the polymerization velocity and the average lengths of attached and detached filaments start to decrease again and the cycle starts anew. The period of oscillations is dependent on the parameter values. It reduces from 240 s in figure 4(a) to 13 s in figure 4(b) as k_a increases from 0.143 to 3.49 s^{-1} at $v_g^{max} = 300\,nm\,s^{-1}$.

The oscillations in x correspond to the saltatory motion of the obstacle since v_g stays essentially constant. An illustration is shown in figure 6, which has the same velocity maxima and period as the experimental data shown in [22], figure 8(b). We found the velocity maxima to be close to v_p^{max}. The velocity between the spikes in the simulations is about 2–3 times larger than the experimental value. We assume this to be caused by neglecting capping. The period of velocity oscillations of beads propelled by actin polymerization differs from those of *Listeria* by one order of magnitude (8−15 min [23]) and velocities are much smaller. These periods and velocities can be obtained within our model with smaller values for v_g^{max} and v_p^{max} (see figure 6(b)). However, experimental oscillations of bead velocities show a peak broader than the simulated ones [23].

As mentioned above, actin density variations in the comet tail of beads and pathogens accompany the velocity oscillations in experiments. These density variations do not occur in our model. This demonstrates that they are not required for the velocity to oscillate. The variations in pulling and pushing forces driving the push–pull mechanism do not arise from density changes but from the length oscillations of attached and detached filaments via the force–extension relations of semiflexible polymers. The push–pull mechanism is not in contradiction to the observed density variations and their phase relation with respect to the velocity time course. Both pulling and pushing forces increase with the filament density. Therefore, the force changes resulting from density variation would not counteract the force changes occurring in our model but probably support and amplify them.

4. Conclusions

In summary, we derived a simple model for velocity dynamics in actin-based motility by starting from the dynamics of length distributions of a free polymer in the brush. We have presented a theoretical description of oscillations arising from the interplay of polymerization-driven pushing forces and pulling forces due to binding of actin filaments to the obstacle. The mechanism relies on the load dependence of the detachment rate and the polymerization velocity. The model uses parameter values determined from measurements. It reproduces the dynamic regimes of actin-based motility observed with obstacles riding on an actin comet tail, the type of bifurcation observed in bead experiments upon an increase in protein concentration and the onset of oscillations in oil droplet motion upon VASP addition. Oscillations are observed for a range of tilt angles of the filaments as required for modeling of actin brushes of experimentally observed actin comet tails.

A recent review by Mogilner distinguishes microscopic models and continuum models [38]. The tethered ratchet model is the prototypical microscopic model since it starts from the properties of individual filaments. Our model belongs to the same group. Velocity oscillations have not been explained yet with microscopic models. Here, we show that this class of models can reproduce oscillations also. In contrast with the tethered ratchet model, equations (9) include dynamics of the lengths x, l_a and l_d. This appears to be the reason why our model oscillates so robustly while the tethered ratchet model shows steady motion only.

An alternative theoretical explanation of *Listeria* and bead propulsion by actin polymerization was given by the continuum model, which perceives the actin meshwork as a continuous gel [22, 23, 37]. It explains the oscillatory motion as a consequence of tangential stress which arises when an actin gel grows from the inside outwards on bent surfaces. Friction arising from the binding of polymers to the surface keeps the velocity small until the stress is released due to bond rupture and a stick–slip transition occurs (soap effect). The dependence of the reaction rates on load leads to a nonlinear relation between friction force and velocity in the quasi-static regime as shown in conjunction with the derivation of the continuum model [22]. However, the catastrophic rupture of attached filaments required for velocity oscillations is not captured by the quasi-static force velocity relation but was assumed to occur at a cut-off value for F_d [22, p 2269]. Here, we show that it occurs indeed as a consequence of the force dependence of the reaction rates.

A way to store elastic energy seems also to be required to obtain oscillations. It is stored in tangential stress of a bent gel in the continuum model [22] and in the tension between pushing and pulling filaments in our model. Consequently, the mechanism of thrust generation during the velocity peaks is different in the two models: soap effect [22] versus push–pull. The oscillations in our model do not require bent obstacle surfaces and are very robust with respect to changes in various parameters, i.e. they appear to be generic. Therefore, complex biochemical regulatory systems supplementing the core process described here may rather stabilize motion and suppress oscillations than generate them. Nevertheless, aspects of the continuum model—like tangential stress—would of course enter our model if curved obstacle surfaces are considered. The formation of tangential stress on curved surfaces provides an explanation for the radius dependence of the onset of oscillations as shown by the continuum model [23]. Since the push–pull mechanism and the soap effect are not clearly mutually exclusive, identifying which of them applies for a specific system would require further specification of the model as well as further experiments.

Acknowledgments

We thank M Enculescu, R Straube and V Casagrande for inspiring discussions. EF acknowledges financial support from the German Excellence Initiative via the program 'Nanosystems Initiative Munich (NIM)'. AG acknowledges financial support from the IRTG 'Genomics and Systems Biology of Molecular Networks' of the German Research Foundation.

References

[1] Mogilner A and Oster G 1996 *Biophys. J.* **71** 3030
[2] Gholami A, Wilhelm J and Frey E 2006 *Phys. Rev.* E **74** 41803
[3] Bray D 2001 *Cell Movements* (New York: Garland)
[4] Plastino J and Sykes C 2005 *Curr. Opin. Cell Biol.* **17** 62
[5] Gouin E, Welch M D and Cossart P 2005 *Curr. Opin. Microbiol.* **8** 35
[6] Loisel T P, Boujemaa R, Pantaloni D and Carlier M F 1999 *Nature* **401** 613
[7] Upadhyaya A and van Oudenaarden A 2003 *Curr. Biol.* **13** R734
[8] Upadhyaya A and van Oudenaarden A 2004 *Curr. Biol.* **13** R467
[9] Marcy Y, Prost J, Carlier M F and Sykes C 2004 *Proc. Natl Acad. Sci. USA* **101** 5992
[10] Parekh S H, Chaudhuri O, Theriot J A and Fletcher D A 2005 *Nat. Cell. Biol.* **7** 1219
[11] Trichet L, Campas O, Sykes C and Plastino J 2007 *Biophys. J.* **92** 1081
[12] Kruse K, Joanny J F, Jülicher F, Prost J and Sekimoto K 2005 *Eur. Phys. J.* **16** 5
[13] Kruse K, Joanny J F, Jülicher F and Prost J 2006 *Phys. Biol.* **3** 130
[14] Joanny J F, Jülicher F, Kruse K and Prost J 2007 *New J. Phys.* **9** 422
[15] Hill T L 1981 *Proc. Natl Acad. Sci. USA* **78** 5613
[16] Cameron L, Svitkina T, Vignjevic D, Theriot J and Borisy G 2001 *Curr. Biol.* **11** 130
[17] Kuo S C and McGrath J L 2000 *Nature* **407** 1026
[18] Mogilner A and Oster G 2003 *Biophys. J.* **84** 1591
[19] Carlsson A E 2003 *Biophys. J.* **84** 2907
[20] Gracheva M E and Othmer H G 2004 *Bull. Math. Biol.* **66** 167
[21] Lasa I, Gouin E, Goethals M, Vancompernolle K, David V, Vandekerckhove J and Cossart P 1997 *EMBO J.* **16** 1531
[22] Gerbal F, Chaikin P, Rabin Y and Prost J 2000 *Biophys. J.* **79** 2259
[23] Bernheim-Groswasser A, Prost J and Sykes C 2005 *Biophys. J.* **89** 1411
[24] Brieher W M, Coughlin M and Mitchison T J 2004 *J. Cell Biol.* **165** 233
[25] Carlier M F and Pantaloni D 2007 *J. Biol. Chem.* **282** 23005
[26] Evans E and Ritchie K 1999 *Biophys. J.* **76** 2439
[27] Co C, Wong D T, Gierke S, Chang V and Taunton J 2007 *Cell* **128** 901
[28] Verkhovsky A B, Svitkina T M and Borisy G G 1999 *Curr. Biol.* **9** 11
[29] Ott A, Magnasco M, Simon A and Libchaber A 1993 *Phys. Rev.* E **48** R1642
[30] Le Goff L, Hallatschek O, Frey E and Amblard F 2002 *Phys. Rev. Lett.* **89** 258101
[31] Wiesner S, Helfer E, Didry D, Ducouret G, Lafuma F, Carlier M F and Pantaloni D 2003 *J. Cell Biol.* **160** 387
[32] Kroy K and Frey E 1996 *Phys. Rev. Lett.* **77** 306
[33] Marko J F and Siggia E D 1995 *Macromolecules* **28** 8759
[34] Biron D and Moses E 2004 *Biophys. J.* **86** 3284
[35] Gov N S 2007 *Europhys. Lett.* **77** 68005
[36] Gholami A, Falcke M and Frey E, unpublished
[37] Gerbal F *et al* 1999 *Pramana J. Phys.* **53** 155
[38] Mogilner A 2006 *Curr. Opin. Cell Biol.* **18** 32